Monthly Notices
of the
ROYAL ASTRONOMICAL SOCIETY

MNRAS **443,** 3712–3727 (2014) doi:10.1093/mnras/stu1376

Dark matter in disc galaxies – II. Density profiles as constraints on feedback scenarios

P. R. Hague★ and M. I. Wilkinson★

Department of Physics & Astronomy, University of Leicester, University Road, Leicester LE1 7RH, UK

Accepted 2014 July 7. Received 2014 July 7; in original form 2014 April 29

ABSTRACT

The disparity between the density profiles of galactic dark matter haloes predicted by dark matter only cosmological simulations and those inferred from rotation curve decomposition, the so-called cusp–core problem, suggests that baryonic physics has an impact on dark matter density in the central regions of galaxies. Using a Markov Chain Monte Carlo analysis of galactic rotation curves we constrain density profiles and an estimated minimum radius for baryon influence, r_1, which we couple with a feedback model to give an estimate of the fraction of matter within that radius that must be expelled to produce the observed halo profile. We examine the rotation curves of eight galaxies taken from the THINGS (The HI Nearby Galaxy Survey) data set and determine constraints on the radial density profiles of their dark matter haloes. For some of the galaxies, both cored haloes and cosmological $\rho \propto r^{-1}$ cusps are excluded which requires finely tuned baryonic feedback. For galaxies which exhibit extended cores in their haloes (e.g. NGC 925), the use of a split power-law halo profile yields models without the unphysical, sharp features seen in models based on the Einasto profile. We have found there is no universal halo profile which can describe all the galaxies studied here.

Key words: galaxies: formation – galaxies: haloes – galaxies: kinematics and dynamics – galaxies: spiral – galaxies: structure – dark matter.

1 INTRODUCTION

Disc galaxies are presumed by ΛCDM cosmology to be dominated by dark matter (e.g. Bosma 1978). An understanding of the arrangement of dark matter is therefore necessary for understanding the kinematics and dynamics of these galaxies. Analysis of galactic rotation curves, as well as of *N*-body cosmological simulations, has produced numerous models describing how dark matter density varies with distance from the centre of a galaxy.

Dark matter-only cosmological simulations were found by Dubinski & Carlberg (1991) and Navarro, Frenk & White (1996) to produce haloes with an approximately universal density profile, with density proportional to r^{-1} towards $r = 0$ and r^{-3} towards $r = \infty$. These haloes follow a set of scaling relations with virial mass such that they behave as a single parameter family of models (Bullock et al. 2001).

The halo density profiles inferred from observing the rotation of disc galaxies appear to contradict this picture. For example, Gentile et al. (2004) inferred the density profiles of five spiral galaxies and found them to be consistent with flat cores. Rotation curves of 17 galaxies analysed by Bosma (2003) were also found to contradict simulations and exclude r^{-1} cusps. This has become known as the cusp–core problem. The possibility of the difference being due to erroneous inference of cores from observations has been discussed, and refuted, in de Blok, Bosma & McGaugh (2003). This, coupled with an increase in resolution of kinematic data, has at this point resolved such concerns.

High-quality data from The HI Nearby Galaxy Survey (THINGS; Walter et al. 2008) have allowed the generation of more detailed rotation curves, that extend to smaller radii than those used in previous treatments of the cusp/core problem (de Blok et al. 2008). An analysis of these rotation curves by Chemin, de Blok & Mamon (2011) showed that an Einasto profile $\rho \propto \exp(-r^n)$, provides a better formal fit than cored profiles such as the Burkert profile (Burkert 1995) or the NFW profile. Also using THINGS data, Oh et al. (2011) claimed that a selection of dwarf galaxies (including DDO 154, which we studied using an MCMC method in Hague & Wilkinson 2013, hereafter HW13) exhibit $r^{-0.29}$ central slopes. They found all the dwarf galaxies in their study to be inconsistent with r^{-1} inner haloes. Velocity fields were also obtained via integral field spectroscopy and used to compare NFW haloes to pseudo-isothermal haloes for 17 galaxies by Kuzio de Naray, McGaugh & de Blok (2008), claiming that a maximal disc and an NFW halo were mutually exclusive.

Simulations have been used to try and resolve the cusp–core problem. Read & Gilmore (2005) demonstrated that the baryon physics left out of pure *N*-body simulations can account for this

★ E-mail: peter.hague@le.ac.uk (PRH); miw6@le.ac.uk (MIW)

disparity, in the case of dwarf galaxies, through time asymmetric mass-loss (e.g. baryon infall and outflow), and Governato et al. (2010) used supernovae feedback to explain both the flattening of the inner dark matter density profile and the absence of bulges in dwarf galaxies. Another approach by Katz et al. (2014) attempted to account for the current density profile of a subset of THINGS galaxy dark matter haloes using only adiabatic contraction. They fit NFW profiles to the rotation curve data from de Blok et al. (2008) and compare the concentration parameter with that of a primordial halo.

In this paper, we attempt to provide an improved modelling of dark matter density profiles in a selection of THINGS galaxies using a more general parametrized density profile, the $\alpha-\beta-\gamma$ profile (Zhao 1996), and a Markov Chain Monte Carlo (MCMC) method to explore the parametrization. We also explore the implications of our improved density profiles for our understanding of feedback processes. The structure of this paper is as follows: Section 2 summarizes the rotation curve decomposition and MCMC techniques used to derive dark matter density profiles. Section 3 describes a simple analytic model that can be used to constrain formation scenarios for an individual galaxy given its halo density profile and rotation curve. Section 4 discusses the results for individual galaxies, and Section 5 draws conclusions from the analysis when applied to our full sample of galaxies.

2 METHOD

The rotation curve analysis method used in this paper is described fully in HW13. Here, we will briefly summarize our data processing chain: first, the method used by de Blok et al. (2008) to derive rotation curves from the THINGS velocity fields; secondly, the halo density profile we fit to these data and the parameter space defined by it; and then finally, the MCMC method that we use to constrain the density profiles of the dark matter haloes. The output of this method is a distribution of halo models, and thus provides not only a best-fitting model but also robust errors.

2.1 Baryonic mass modelling

The rotation curve decompositions we used were provided by de Blok, and we describe their generation here for completeness. A more thorough description can be found in de Blok et al. (2008). Data from the *Spitzer* Infrared Nearby Galaxy Survey (SINGS; see Kennicutt et al. 2003) provide surface brightness data that, when mapped on to tilted rings and combined with an estimate of the mass-to-light ratio Υ for the stellar population, can give a radial mass distribution for the stellar component of the galaxy. When modelling 1D rotation curves, we assume that it is sufficient to model this as an axisymmetric disc with exponentially decreasing density as a function of radius.

In de Blok et al. (2008), two values are used for Υ: one derived from a Kroupa initial mass function (IMF) and one derived from a version of the Salpeter IMF with the mass reduced by 30 per cent that is referred to as a diet Salpeter IMF. Bell & de Jong (2001) found that reducing the number of low-mass stars relative to the original Salpeter IMF was required in order to make the stellar disc 'consistent with the maximum disc constraints'. We use this value for Υ only as a centre point for the parameter range, half a dex either side of the values given in table 3 in de Blok et al. (2008), which in all cases besides DDO 154 (due to its very low surface brightness) already encompasses baryonic mass scalings up to, and including, a maximal disc.

Gas can be modelled in the same way, from the THINGS data, but there are fewer issues determining the mass of gas present. H I emission is proportional to the neutral hydrogen present, and a scaling factor of 1.4 is applied that takes into account the amount of helium and metals that will also be present. Again, an exponential disc model is used in order to generate an axisymmetric potential and thus a 1D rotation curve contribution.

Our models do not include molecular gas, but following the method of de Blok et al. (2008) we assume that the density distribution of this gas follows that of the stars and is a small fraction of the stellar surface density. There would be no benefit of introducing a parameter describing the ratio of stars to molecular gas, as it would be entirely degenerate with Υ.

There is some uncertainty in the inclinations of the galaxies studied here, which would manifest itself in a rotation curve as a systematic shift in the circular velocity. It would be possible to include the inclination as a parameter in our study; however, it would also be degenerate with Υ; stellar and gas mass modelling are insensitive to inclination unless significant extinction occurs. This can only happen when the galaxy is near to edge-on, and the galaxies in our set have already been selected to have intermediate inclination (see de Blok et al. 2008).

2.2 Dark halo profiles

We make three assumptions about the dark matter haloes of the galaxies analysed in this paper:

(1) They are spherically symmetric.
(2) The density monotonically decreases with radius.
(3) The log slope is continuous and differentiable with respect to radius.

Satisfying these constraints, a general, spherically symmetric, halo density profile has been selected, which either analytically encloses, or closely emulates, all commonly used density profiles. We start with the $\alpha-\beta-\gamma$ profile (Zhao 1996)

$$\rho(x) = \frac{\rho_s}{x^\gamma(1+x^{1/\alpha})^{\alpha(\beta-\gamma)}}, \quad (1)$$

where ρ_s is the scale density, r_s is the scale radius and α, β, and γ are shape parameters. γ determines the log slope at $r = 0$, β determines the log slope as $r \to \infty$ and α the rate at which the profile transitions between the two power laws, with lower values being a sharper transition. We transform the parameter space of this profile; thus,

$$\rho(x) = \frac{\widetilde{\Sigma}_{\rm max}}{G}\frac{v_{\rm max}^2}{x^\gamma(1+x^{1/\alpha})^{\alpha(\beta-\gamma)}}, \quad (2)$$

where $x = r/r_s$, with r_s the scale radius, $v_{\rm max}$ is the peak velocity of the dark matter rotation curve and $\widetilde{\Sigma}_{\rm max}$ is given by

$$\widetilde{\Sigma}_{\rm max} = \frac{\rho_s r_{\rm max}}{M(r_{\rm max})}, \quad (3)$$

where $r_{\rm max}$ is the radius at which the profile's rotation curve reaches its maximum velocity, $M(r_{\rm max})$ is the mass enclosed at that radius. A derivation and more complete description of this can be found in HW13. The degeneracy removed by our transformation can be seen in fig. 1 of Katz et al. (2014), the case of an NFW profile (a subset of the $\alpha-\beta-\gamma$ halo) which applies a similar Monte Carlo method to ours to a simpler parameter space.

Because double power laws with respect to radius can be approximately modelled (provided the transition between the two powers

is smooth) by a single power law over a finite range, we assert that our two power models can represent any profile containing more power laws, over a finite radial range, as long as a similar condition of smoothness is met.

2.3 Markov Chain Monte Carlo

An MCMC method (Hastings 1970) is used to integrate over the parameter space defined by the profile given in equation (2) along with two disc scaling parameters; a mass-to-light ratio multiplier f_Υ which scales the magnitude of the stellar contribution (relative to the mass-to-light ratio Υ for the diet Salpeter IMF case in de Blok et al. 2008). We consider f_Υ in the range [0.316, 3.16] which encloses the Kroupa IMF and the factor of 2 variation in infrared IMF suggested by Bell & de Jong (2001). We use COSMOMC (Lewis & Bridle 2002), in a generic mode, together with a likelihood function of our own as our MCMC engine. MCMC is a Bayesian method that generates a probability distribution in the parameter space of a set of models. Bayes' Theorem states that

$$P(M[\boldsymbol{x}]|D) = \frac{P(D|M[\boldsymbol{x}])P(M[\boldsymbol{x}])}{P(D)}, \tag{4}$$

where M is a proposed model defined by parameter vector $\boldsymbol{x}$, and D is the data. Assuming that $P(D) = 1$, we can then generate a series of values for $P(D|M)$ via a Markov chain process. Starting at a random point, the algorithm generates a new candidate point based on a random step drawn from a probability distribution, which in this case we take to be Gaussian. The new point $\boldsymbol{x}'$ is added to the Markov chain with a probability

$$P_{\rm accept} = \min\left[\frac{P(D|M[\boldsymbol{x}'])}{P(D|M[\boldsymbol{x}])}, 1\right] \tag{5}$$

if the new point is not accepted, the current point is added again to the Markov chain. This process is repeated and, provided the chain is able to converge, produces a distribution of $P(D|M[\boldsymbol{x}])$, which can be combined with the prior distribution $P(M[\boldsymbol{x}])$ to calculate the probability distribution we seek.

A condition required for an MCMC run to converge well is that the step size (measured in our Gaussian case by a standard deviation σ in each parameter) is appropriate to the distribution. This can either be done by trial and error, or by a step size that adapts during the course of the run. We opt for the second approach, updating the probability distribution of candidate points relative to the current point based on a covariance matrix generated from the most recent half of the models generated. COSMOMC then samples $P^{1/T}(D|M[\boldsymbol{x}])$, where T is a temperature value which we set equal to 1 (reducing to equation 5) unless there are specific problems finding a constraint, where we use $T = 2$.

A further condition for convergence is that the parameter space be able to cover the entire range of models that are likely to fit the data. In our case, this condition is of most concern for those haloes where $\gamma \to 0$, which are required to model the flat-cored Burkert (1995) halo. Boundary effects at the edge of the parameter space not only cause problems integrating there due to cutting off part of the Gaussian selection function, but also necessarily mean that the distribution is not normalized. Strictly, MCMC produces a non-normalized distribution, but the distribution can be normalized correctly if the probability tends towards zero at the boundaries of the parameter space, and the distribution can be assumed to have no models with non-zero probability outside this space.

To resolve this boundary issue, we mirror the parameter space around $\gamma = 0$. The MCMC explores a parameter range γ' in the range $[-2, 2]$, and generates parameter values using $\gamma = |\gamma'|$, so the actual parameter γ is only explored in the range [0,2]. We do not consider negative values of γ physically consistent with our model of the dark matter halo.

We use eight independent MCMC chains, each using approximately 5×10^6 models (the code terminates once the first chain completes, but as the run time for the chains is quite consistent this does not usually cause the chains to be unduly shortened). The first 1×10^5 models in each chain are treated as burn in, the process by which the MCMC algorithm initially finds and moves into the main body of the distribution, and discarded.

Previous work on rotation curves such as Chemin et al. (2011) and Oh et al. (2011) has tested a small number of proposed density profiles against the data; these profiles represent single points (or in the case of the Einasto profile, curves) within the parameter space we explore. By fully characterizing the parameter space, we are able to put these previous fits in a wider context.

3 ANALYSIS

Once we have generated distributions of density profiles for each galaxy, we investigate their systematic properties, with reference to previous claims regarding the nature of dark matter haloes. Our primary focus is to find properties of the dark matter haloes that could constrain formation scenarios.

In previous work (see e.g. van den Bosch & Swaters 2001), haloes whose density profiles became flat as $r \to 0$ are referred to as 'cored', whereas haloes that show density profiles approaching $\rho \propto r^{-n}$ where $n \geq 1$ are referred to as cusped. Terminology for intermediate haloes (i.e. those with $0 < n < 1$) is unclear. For the purposes of our discussion, we consider such haloes neither fully cusped nor fully cored.

The parameter γ, the asymptotic log slope of the profile as $r \to 0$, is a property of the profile that describes the shape of the halo outside the data range. Therefore, we generate, from the halo profiles, an alternative parameter $\gamma_{\rm in}$. This is the log slope of the dark matter halo density profile at the innermost data point of the measured rotation curve. As the data sets all start at a different radius, direct comparisons between galaxies using $\gamma_{\rm in}$ are not possible. It is, however, a useful quantity because if it is substantially above zero, it excludes the existence of a core within the data range.

Another value we extract from our density profiles is r_1. This is the radius at which the log slope (which must monotonically decrease for all profiles) reaches -1. As we will show, this a well-constrained and useful scale radius.[1] In order to demonstrate its utility, we construct a simple model for the formation of the galaxies we study here.

If we assume that the starting point for a dark matter halo is an NFW profile (or some other cosmological profile that tends towards a log slope of -1 at $r = 0$), then the density profile must have a logarithmic slope of $\mathrm{d}\log\rho/\mathrm{d}\log r = -1$ or steeper at all radii, so any part of the density profile that has a shallower slope can clearly be stated to be inconsistent with a cosmological profile derived from pure dark matter N-body simulations. Thus, r_1 gives us a radius to which the effects of any process which modifies the shape of the

[1] In some work (e.g. Chemin et al. 2011), the radius r_2 is also used (sometimes written as r_{-2}, but we exclude the sign in order to maintain consistency with the positive sign of the parameters in the $\alpha-\beta-\gamma$ profile). For individual profiles (such as Burkert profiles) the relationship between these is a straightforward, constant ratio.

halo must reach in order to account for the current density profile, and we now show that this is a conservative estimate.

The choice of the parameter r_1 is based on the minimization of assumptions. To construct an exact model of an observed galaxy at the time of its formation would require knowledge of the density of the Universe and assert the exact correctness of a particular halo model such as NFW or Einasto (whereas we only assume that the halo had a cusp of some kind). Using r_1 allows a degree of physical modelling without having to resolve these unknowns.

In order to investigate the origins of non-cosmological (i.e. $\gamma < 1$) haloes, we construct a simple model of feedback, where outflows of gas on time-scales shorter than the dynamical time of the halo can impart energy to the halo and alter its density profile. The source of this feedback can either be an accreting central black hole, supernovae, or other stellar feedback.

Our model features an inhomogenous spheroid of gas in a spheroid of dark matter, and a disc. Gas is removed entirely from the galaxy instantaneously and permanently during an outflow (realistic, given velocities of various possible outflows in e.g. Governato et al. 2010; King 2003). Spheroidal symmetry allows us to make a number of simplifying assumptions in the discussion which follows in both the spherical case, and the oblate spheroidal case (Binney & Tremaine 2008). Hereafter, we only discuss radius, however the arguments still apply using the equivalent coordinate in an oblate spheroidal system.

Given the assumed geometry, dark matter particles can only respond to changes in the mass interior to their current position. If a certain portion of this mass is removed, a particle will respond by moving outwards. Assuming a much longer time-scale for the removed mass to fall back in (if it does at all) the upper limit to the instantaneous change in the total energy of dark matter particles at any particular radius, taking the potential to be relative to r_1 is the change in potential interior to that radius. As baryons and dark matter move in the same potential, we assume a mass of baryons outflowing past r_1 can bring the same mass of dark matter with it. The change in dark matter mass of the halo interior to r_1 is obtained from

$$M_{\mathrm{I,dark}}(r_1) = M_{\mathrm{F,dark}}(r_1)(1 - f_{\mathrm{b}})^{-1}, \quad (6)$$

where $M_{\mathrm{I,\,dark}}(r)$ is the initial mass interior to r and f_{b} is the fraction of mass that is in baryons and thus available for an outflow. We assume that the available gas is arranged in a diffuse spheroid, follows the density profile of the dark matter. In this case, we are modelling a single outflow, or multiple outflows where any gas falling back in negates the effects of its initial outward movement exactly. In reality, infall happens over a much larger time-scale than outflow (see e.g. Governato et al. 2010), but modelling this is beyond the scope of the simple model we are constructing here, and will be addressed in later work.

We assume here that the amount of dark matter removed from inside a radius r is approximately equal to the amount of gas removed. To verify this, we ran a series of 2×10^6 particle N-body simulations using FALCON (Dehnen 2000, 2002), using spherical initial haloes with inner log slopes $\gamma = 0, 0.25, 0.5, 7/9, 1$, and removing a fraction of mass equal to $f_{\mathrm{b}} = 0.02, 0.04, 0.08, 0.16, 0.24, 0.48, 0.64, 0.90$. Mass is removed equally from all of the particles in the simulation. Under conditions of spherical symmetry this does not produce a different result from removing all the mass interior to r_1, and does not require an extra step of calculating the position of r_1.

We compared mass before and after, within the scale radius, and found that for a cosmological baryon fraction, the fraction of dark matter carried away with gas outflow is of order unity, as shown in Fig. 1.

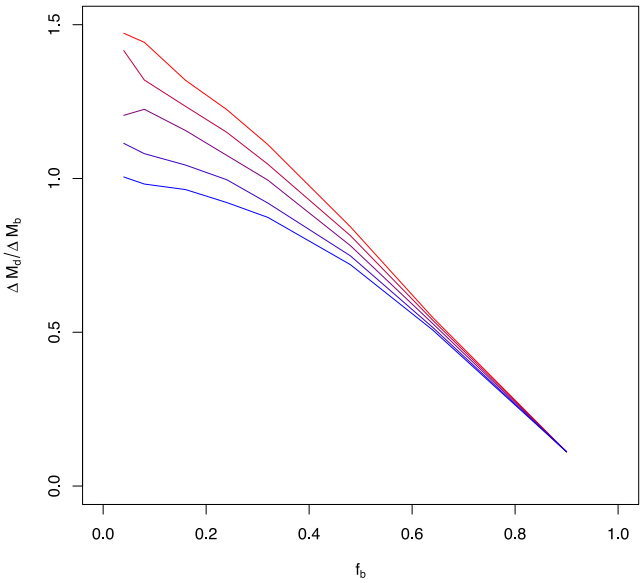

Figure 1. Ratio of expelled dark matter ΔM_{d} to expelled baryons ΔM_{b}, from N-body simulation, for a range of initial conditions. Red to blue denotes increasing log slope (0, 0.25, 0.5, 7/9, 1). Simulations were run for baryon fractions $f_{\mathrm{b}} = 0.02, 0.04, 0.08, 0.16, 0.24, 0.48, 0.64, 0.90$. Deviations of the curves at low f_{b} are due to ΔM_{b} being a smaller multiple of M_{particle}.

The starting conditions for these simulations were constructed in equilibrium using MKHALO from the same software suite – in reality the response of the dark matter to gas outflow is dependent on the velocity structure of the halo. This velocity structure depends on the precise history of the halo, as shown in Read & Gilmore (2005) where halo cores are formed by moving particles from tangential to radial orbits. Thus, the exact order of the curves in Fig. 1 should not be taken as strictly realistic, but it does demonstrate that the ratio between the dark matter removed and the gas removed at a certain radius should be of order unity.

From equation (6), assuming an initial and a final mass profile, we can compute the spheroidal baryon content at the time the outflow(s) occurred. In reality this could be raised by contraction of the gas content of the galaxy, or lowered due to baryons leaving the spheroidal gas component through either clumping, or becoming part of the disc, and either way being too dense to participate in an outflow event. However, we are able to produce a consistent model to predict f_{g} – the fraction of matter available as gas of sufficiently low density to be part of the feedback process.

Assuming the dark matter halo mass interior to the outermost data point, we have observed is unchanged through feedback, there exists an NFW profile (using the scaling relation established in cosmological simulations) that gives a value for $M_{\mathrm{I}}(r_1)$ and the model above then gives f_{g}. In Section 5, we determine this value for this set of galaxies, and discuss whether they are realistic.

4 RESULTS

Table 1 shows relevant physical information for the galaxies in our sample and some detail of the MCMC output. We have sampled 4×10^7 models in each case, using eight independent MCMC chains which have converged to similar distributions. The quantitative convergence statistic we use here, provided by the GETDIST

Table 1. Galaxies studied in this paper, ordered by absolute B magnitude. (1) Maximum circular velocities taken from rotation curves. (2) Amplitudes of non-circular motions, in the inner 1 kpc of each galaxy, from Trachternach et al. (2008). NGC 3198 only has one data point inside this radius so no bounds are available. (3) Absolute B magnitude from Walter et al. (2008). (4) Molecular gas to atomic gas ratio, calculated from HERACLES data (Leroy et al. 2009), where available. (5) The number of models sampled, excluding a burn in of 10 000 models in each of eight chains. (6) The temperature parameter used with COSMOMC, which samples $P^{1/T}$ of each model. (7) Largest (i.e. worst) value of the statistic used to check that chains are converged on to the same likelihood distribution. See text for details.

Galaxy	$V_{\rm c,max}$ (km s^{-1}) (1)	$A_{\rm r,1kpc}$ (km s^{-1}) (2)	Absolute B magnitude (3)	H II/H I ratio (4)	Models (5)	T (6)	$\sigma(\hat{x})/\hat{\sigma}(x)$ (7)
DDO 154	53.28 ± 3.79	$1.43\pm^{0.14}_{0.53}$	−14.23		38 880 635	1	0.0085
NGC 2976	86.23 ± 3.46	$2.18\pm^{0.77}_{0.55}$	−17.78	0.36	39 310 884	1	0.0098
NGC 7793	117.6 ± 5.0	$3.41\pm^{0.64}_{0.48}$	−18.79		39 539 819	1	0.0529
NGC 2403	143.9 ± 4.5	$2.60\pm^{0.59}_{0.48}$	−19.43		34 880 553	2	0.1315
NGC 925	114.5 ± 7.4	$9.45\pm^{0.64}_{2.98}$	−20.04	0.04	38 180 473	1	0.0959
NGC 3621	157.0 ± 5.7	$5.52\pm^{0.94}_{3.21}$	−20.05		38 025 138	1	0.3916
NGC 3198	158.7 ± 3.2	1.50	−20.75	0.04	36 688 012	1	0.3113
NGC 3521	218.8 ± 28.0	$3.12\pm^{12.67}_{1.77}$	−20.94	0.38	36 845 437	2	0.7693

program which accompanies COSMOMC, computes the variance of the means of the chains $\sigma(\hat{x})$, divided by the mean of the variances of the chains $\hat{\sigma}(x)$, and must be smaller than unity for a set of chains to be converged. This statistic is calculated for each parameter, and the largest value is taken to be an overall measure of convergence.

The galaxies we study are modelled by de Blok et al. (2008), utilizing H I velocity maps from THINGS to derive the rotation speed, the same H I data to derive a radial gas density profile, and 3.6 μm maps from SINGS (along with assumed Υ ratios) to derive the stellar components. Some of the galaxies in this sample are modelled with a single stellar disc, whilst some are modelled with a stellar disc and a separate bulge component.

Fig. 2 shows the distribution of halo log slope profiles for all accepted models in the MCMC chains. We categorize as having cored haloes NGC 925, NGC 3198, NGC 3521 and (with a weaker constraint) NGC 2976. We find cusps in NGC 2403 and NGC 3621, and intermediate inner log slopes in DDO 154, NGC 3198 and NGC 7793. Fig. 3 shows the rotation curve decomposition of the most populated bin of parameter space in the MCMC chains.

4.1 DDO 154

This is the least massive galaxy in the set we are examining, having a mass of 3×10^9 M$_\odot$ according to Carignan & Purton (1998), and thus has lower rotation speeds overall than the other galaxies. Given that its low surface brightness makes the dark matter halo parameters easier to constrain, we used it as a test case for the method that we discussed in HW13. That paper contains some analysis of the result.

The H I velocity field of this galaxy is asymmetric in the outer parts (illustrated in fig. 81 in de Blok et al. 2008), but as we are concerned mainly with the potential at small r, this is not an obstacle to the constraint of $\gamma_{\rm in}$. The rotation curve is well constrained and, based on the errors which are calculated from the difference between the two sides of the rotation curve, quite symmetrical in the region of interest. We find a well-constrained $\gamma_{\rm in}$ value, with an intermediate log slope at the innermost data point ($r = 135.7$ pc). Unsurprisingly this value is unaffected by the chosen value of f_Υ due to the low contribution of the stellar disc to the rotation curve.

In HW13, the gas curve for this galaxy was represented by the rotation curve of a smooth exponential disc. We have opted to no longer do this, first because the gas contribution does not significantly alter the result anyway, and secondly, because any smoothing that is necessary should be handled by the MCMC process. We now directly use the gas velocity data from de Blok et al. (2008). This reasoning is supported by the fact that we indeed get the same value for $\gamma_{\rm in}$, within error, as that reported in HW13.

4.2 NGC 2403

The data for this galaxy have large error bars relative to their scatter (fig. 70, de Blok et al. 2008). However, we demonstrated in HW13, using test data, that our method is robust to this issue.

The constraint on the inner log slope is shown in Fig. 4. With a freely varying mass-to-light ratio, the distribution of $\gamma_{\rm in}$ is clearly not Gaussian, showing a plateau towards more cored values. This part of the parameter space is noisy, and the level of the noise is not consistent across parameter space. Whilst formally converged ($\sigma(\hat{x})/\hat{\sigma}(x) = 0.73$), the presence of the plateau reveals something interesting about the parameter space, as well as pointing to the need for judicious use of convergence statistics. The peak at the high end of the $\gamma_{\rm in}$ distribution appears in all chains. Fig. 5 shows that the inner log slope has a single smooth peak when f_Υ is fixed by assuming either a diet Salpeter or Kroupa IMF, in both cases consistent between chains, indicating that the additional tail in the free f_Υ case is due to a degeneracy (shown in Fig. 4) between the dark matter halo parameters and the mass-to-light ratio. This is to be expected for a higher surface brightness galaxy – at higher values of f_Υ, the stellar contribution is able to model the rotation curve alone, and the MCMC then finds fits with low dark matter density where the exact shape of the halo is less important.

The small, cored plateau represents models which attempt to fit maximal disc models to the data, and such models require very high values of f_Υ. Furthermore, the fact that these models cannot form a second peak in the distribution indicates that they do not reproduce the data as well as those in the peak. We now explore this in more detail. The maximal disc part of parameter space occupies a large volume, due to the fact that the shape parameters of the dark matter halo are no longer significant, and can be freely varied without compromising the quality of the fit. This can bias the MCMC chains towards that volume, so if models there were of a higher fitness than those in the peak, the plateau region would be strongly favoured in all chains. If we disregard these models on this basis, we can conclude that NGC 2403 has a moderate cusp. As shown in Fig. 5,

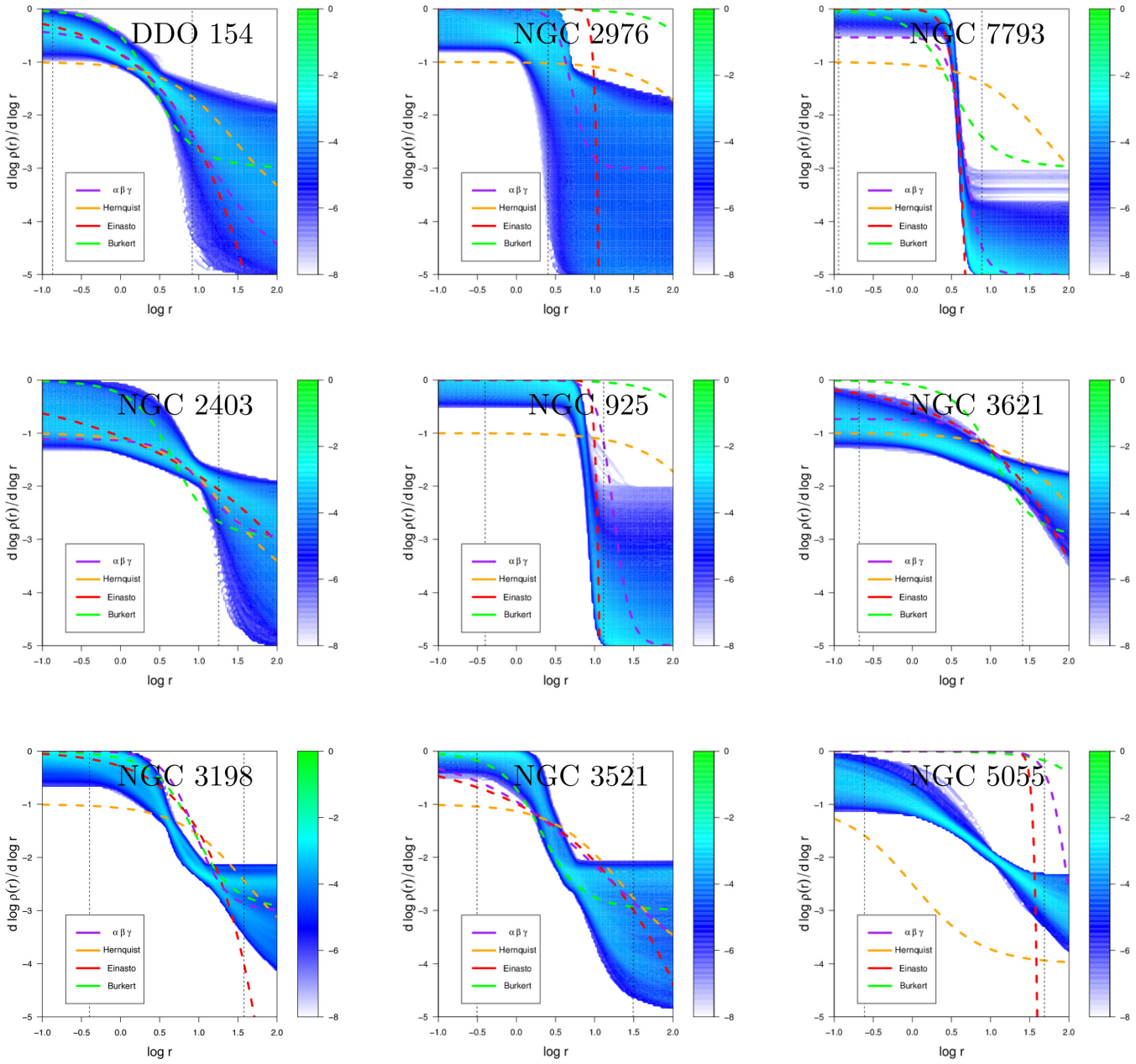

Figure 2. Overlay of all models produced by the MCMC algorithm for each galaxy, in log$r$−d logρ/d log$r$ space. The log density scale on the right of each plot is relative to total number of models. Vertical dotted lines indicate the radial range of the observed rotation curve data, with the inner limits for NGC 2976 and NGC 2403 being below log$r = -1.0$. Dashed curves are least squares minimization fits of common density profiles (Green: Burkert profile. Orange: Hernquist profile. Purple: $\alpha-\beta-\gamma$ profile. Red: Einasto profile). NGC 5055 is included for comparison although it is one of the galaxies rejected from our analysis. See text for a detailed discussion.

a cusp is also indicated when using a fixed f_Υ derived from either Kroupa or diet Salpeter IMF.

We took a subsample of 1423 models from the MCMC chain, that were randomly selected after burn-in with a probability of 10^{-4} for each model, and then divided this into two subsamples either side of $\gamma_{\rm in} = 0.5$. We found no difference in reduced χ^2 for either side, to two significant figures. Both produced a 90 per cent confidence interval of $\chi^2_{\rm red} = 0.30, 0.31$. Given the very definite preference of the MCMC chain, and the fact that values of $\chi^2_{\rm red} < 1$ are of little use for comparison, we conclude that the algorithm is still able to produce a meaningful result. We also note that the number of degrees of freedom is treated as a constant when using $\chi^2_{\rm red}$, but the nature of the problem means that in some parts of the parameter space not all of the parameters contribute significantly to the fit – for example, if $v_{\rm max}$ is low and f_Υ is high then the shaping parameters of the dark matter halo can be freely varied whilst maintaining a nearly constant proposed rotation curve. This inherent weakness in $\chi^2_{\rm red}$ does not apply to our MCMC method, as we use the ratio between a proposed model and the current one to determine the next step in the chain, and thus $\chi^2_{\rm red}$ is equivalent to χ^2 (which we use) as the degrees of freedom cancel.

In order to try and produce a better convergence for the tail, we reran the MCMC algorithm using a temperature $T = 2$ (and thus sampling $P^{1/2}$ rather than P). The result was more consistent across

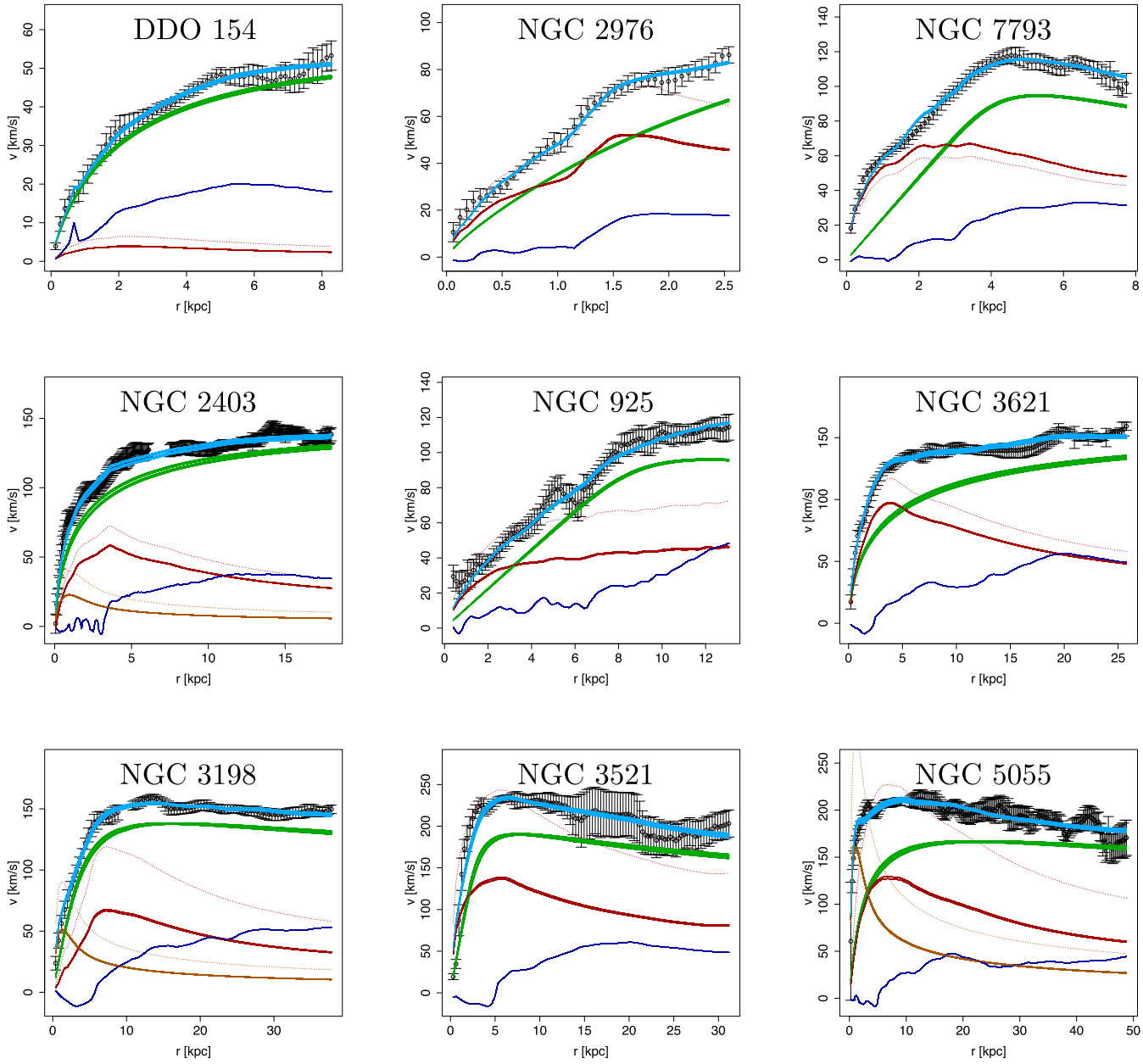

Figure 3. Rotation curve decompositions showing the dark matter haloes corresponding to the most populated bin in the parameter space distribution. Black points represent the observed H I circular velocities, the dark blue curves are the inferred contribution of neutral atomic gas, the solid red curve is the stellar contribution in the best-fitting bin, the dotted red curve is the input value for the stellar contribution (which assumes a diet Salpeter IMF), the green curve is the dark matter contribution and the light blue curve is the resulting combined curve. The green and light blue curves have a thickness as they are the superposition of multiple models in the most populated bin. Two stellar curves are present in NGC 2403, NGC 3198 and NGC 5055 as these galaxies were modelled with two stellar components in de Blok et al. (2008).

independent chains, and produced a smoother distribution overall when the chains are summed, as shown in Fig. 6. This produces the same constraint on $\gamma_{\rm in}$ within 1σ errors. The numeric values discussed in later sections are derived from this version.

4.3 NGC 2976

This galaxy has a high surface brightness, so is not expected to produce as strong a constraint on the dark matter halo as some of the other galaxies have done. This is borne out by the $\gamma_{\rm in}$ distribution in Fig. 7.

As shown in Fig. 3, the rotation curve data for NGC 2976 show a sharp increase just outside 2 kpc, and it is possible to get a mathematically credible fit to the data without treating this as a feature at all. However, the shape of the stellar contribution to the rotation curve suggests that this is the region where dark matter should begin to dominate. Interior to this, the rotation curve follows the features of the stellar contribution well. Therefore, an adequate fit (from the perspective of χ^2 only) can be obtained using $f_\Upsilon \geq 1$ and ignoring the last few data points.

We find, however, that MCMC selects lower values of f_Υ that are able to fit the entire range of data using both dark and visible

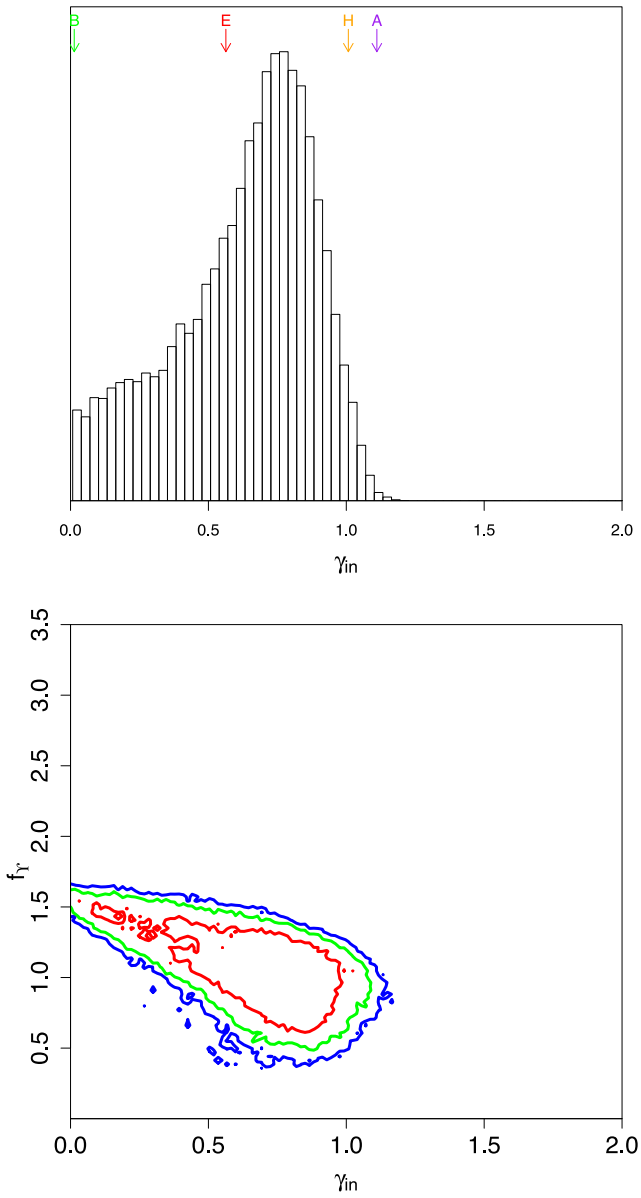

Figure 4. Top: histogram of $\gamma_{\rm in}$ values produced by the MCMC analysis of NGC 2403 with a freely varying mass-to-light ratio multiplier (f_Υ). Arrows indicate the logarithmic slope at this radius of single profile fits (Green: Burkert profile. Orange: Hernquist profile. Purple: $\alpha - \beta - \gamma$ profile. Red: Einasto profile). Bottom: contour plot of f_Υ versus $\gamma_{\rm in}$ demonstrating the nature of the degeneracy between the two parameters. The red contour encloses 0.68 of all models in the MCMC chains, the green contour encloses 0.95 and the blue contour encloses 0.99.

components, as shown in Fig. 3. The free f_Υ run gives $r_1 = 1.94 \pm^{1.76}_{0.4}$ (90 per cent confidence), which has an upper bound outside the data range. The lower bound roughly corresponds to the point where the contribution to the circular velocity from the dark matter halo first exceeds that of the stellar disc.

4.4 NGC 3198

This galaxy has a well-studied rotation curve (e.g. Begeman 1989). Error bars show the disc is roughly axisymmetric, and there are good kinematic data from the H I map at all radii (fig. 75 in de Blok et al. 2008).

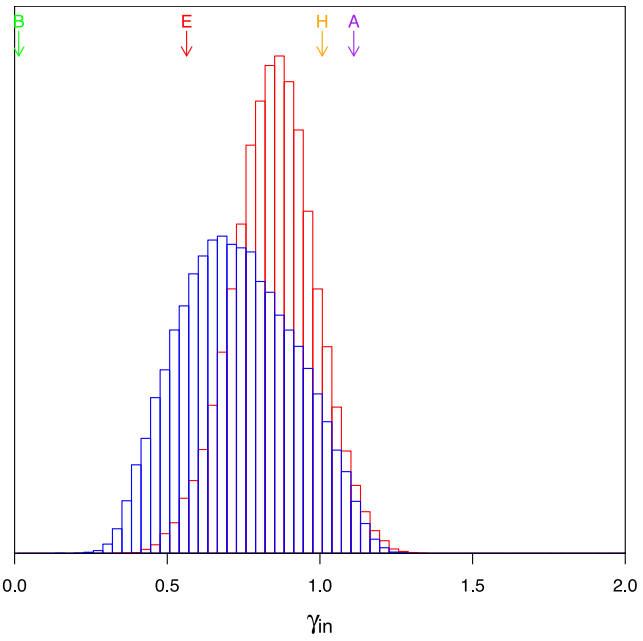

Figure 5. Histograms of $\gamma_{\rm in}$ values produced by MCMC analyses of NGC 2403 with fixed stellar IMF. Blue: with a fixed f_Υ derived from a diet salpeter IMF. Red: with f_Υ derived from a Kroupa IMF (Kroupa 2001). Arrows are as in Fig. 4.

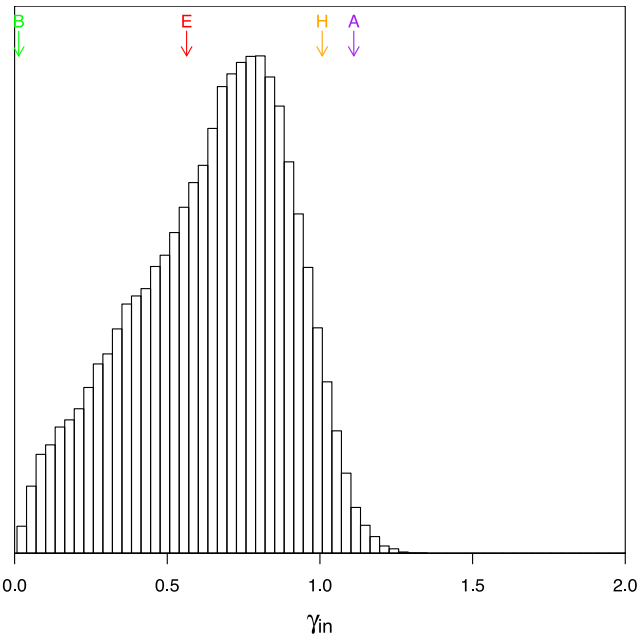

Figure 6. Top: histogram of $\gamma_{\rm in}$ values produced by the MCMC analysis of NGC 2403 with a freely varying mass-to-light ratio multiplier (f_Υ), and a temperature $T = 2$. Arrows are as in Fig. 4. See text for detailed discussion.

One notable feature of the rotation curve for NGC3198 is that the circular velocity contribution of atomic gas is less than zero in the inner part. This represents a void where the net gravitational effect of the gas disc is outwards, and has to be subtracted in quadrature rather than added. This occurs in the same region as the peak of the inner stellar component in the rotation curve, so if the lack of atomic gas could indicate a large amount of molecular gas in the disc (observations of which are not part of any of the original

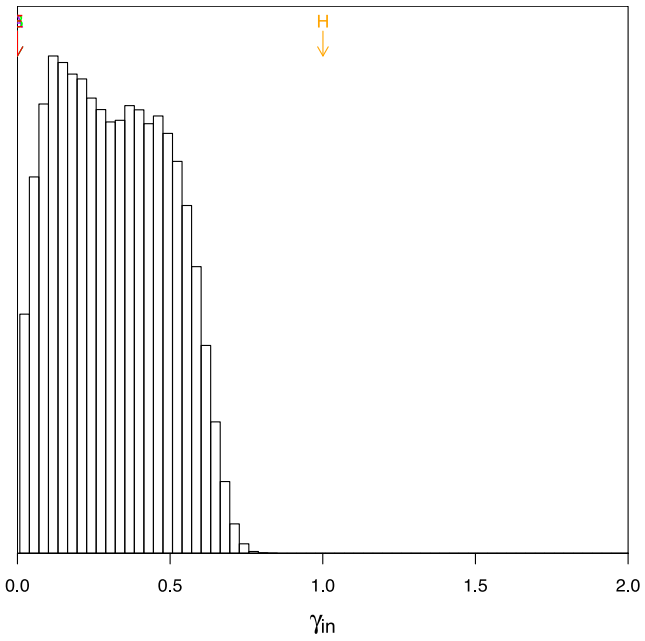

Figure 7. Histogram of the $\gamma_{\rm in}$ value of all the models produced by the NGC 2976 MCMC run. Arrows are as in Fig. 4.

data sources used here), then the contribution of such gas can be modelled by the freedom in f_Υ. Under this assumption, f_Υ no longer functions purely as a factor of stellar mass-to-light ratio.

NGC 3198 is another high surface brightness galaxy, but this itself does not preclude a constraint. The initial run produced differing constraints for each chain, as did a run using the higher temperature setting $T = 2$, but we were able to produce a consistent constraint by also excluding those data points where the neutral gas contribution is negative – which also includes the supermaximal inner stellar component. This constraint had a γ peak greater than 1, and thus no meaningful value for r_1.

Constraints at $T = 1$, using the entire data range, were possible using a fixed f_Υ, with the results shown in Fig. 8. As these both produce constraints on $\gamma_{\rm in}$ that agree to within 1σ, we classify this galaxy as having a core, but this assumes that the stellar mass-to-light modelling is robust. The models produced by the free mass-to-light multiplier run are almost entirely (>88 per cent) below $f_\Upsilon = 0.341$, indicating that the MCMC prioritizes keeping the stellar contribution low in order to keep the inner part of it lower than the observed circular velocity of the galaxy. Better stellar mass modelling is required for a more definitive constraint.

4.5 NGC 3521

We used a temperature setting of $T = 2$ for this galaxy as the lower temperature run produced a constraint value of $\sigma(\hat{x})/\hat{\sigma}(x) = 2.91$ for β. Due to the nature of the data, and the area of our interest being the central region of the galaxy, having a poorly constrained outer log slope is not in itself grounds for a rejecting a result, but in this case both α and $r_{\rm s}$ also had $\sigma(\hat{x})/\hat{\sigma}(x) > 1.0$ when $T = 1$, so we only present the higher temperature run here.

A preference for a core is obtained, as shown in Fig. 9, being flat to within reasonable error at the innermost data point. This remains unchanged regardless which of our initial assumptions about stellar mass-to-light is used, although in the cases of fixed IMF the dark matter contribution is negligible at the smallest radial bin ($r =$

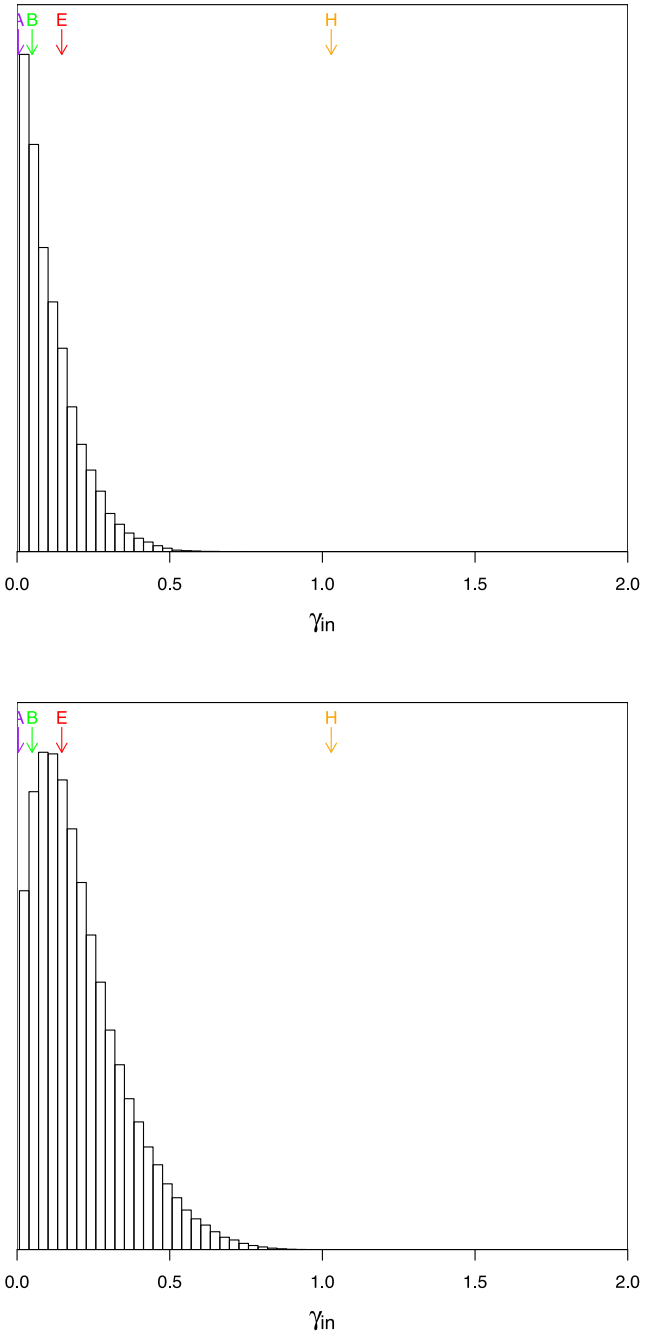

Figure 8. Histogram of the $\gamma_{\rm in}$ value of all the models produced by the NGC 3198 MCMC run using fixed f_Υ. Top: results derived from a Kroupa IMF, and bottom: results derived from a diet Salpeter IMF. Arrows are as in Fig. 4.

312 pc). A strong constraint is however produced on r_1 as shown in Fig. 10. There is no dependence of r_1 on f_Υ, which is also strongly constrained, in the free mass-to-light case. However, the exact value that r_1 is constrained to changes if we use a fixed f_Υ based on a Kroupa or diet Salpeter IMF. This is discussed further in Section 5.

The rotation curve decomposition for NGC 3521, shown in Fig. 3, indicates a gap in the neutral atomic gas disc and also a stellar contribution that is larger than the total rotation curve for the input value of f_Υ, corresponding to a diet Salpeter IMF. Only using the data in the range where the neutral gas contribution to the rotation curve is positive would not permit modelling of the density profile

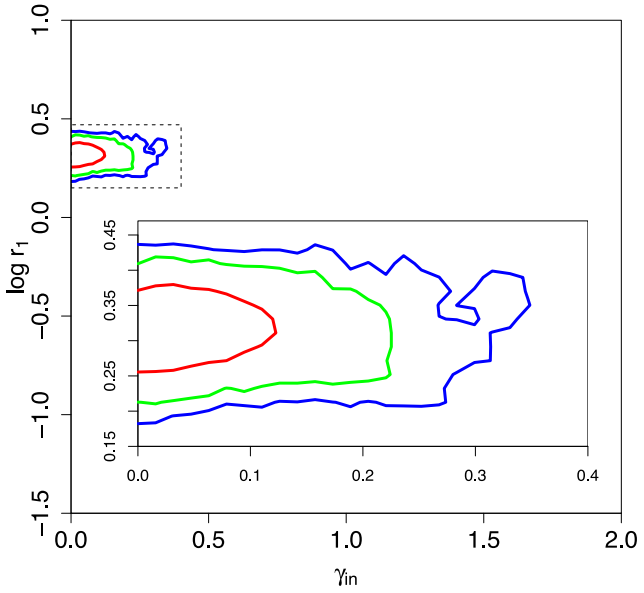

Figure 9. Contour plot of log r_1 versus $\gamma_{\rm in}$ for NGC 3521. Inset shows a zoom in on the contoured region.

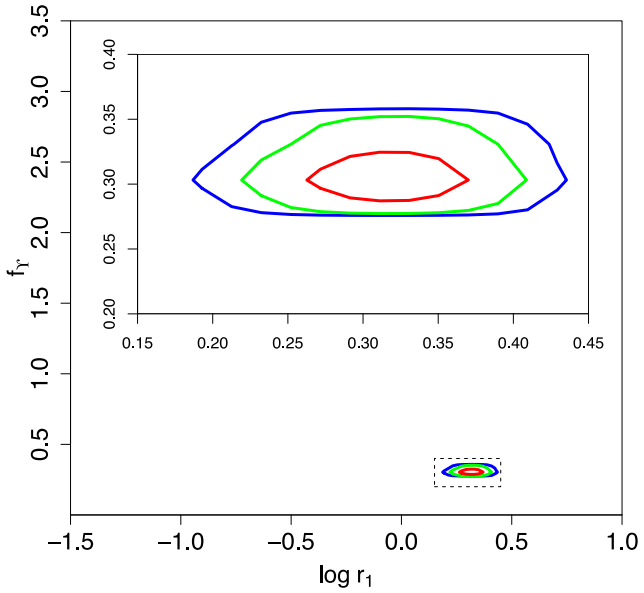

Figure 10. Contour plot of the mass-to-light multiplier f_Υ versus r_1 of all the models produced by the NGC 3521 MCMC run.

shape as all the contributions and the observed rotation curve in the remaining region is almost flat. The rising part of the dark matter halo contribution to the rotation curve is required in order to differentiate between a central core and a cusp. An MCMC run excluding the data points where the velocity of the gas contribution is negative produced a peak $\gamma_{\rm in} \geq 2$, but as stated above this cannot be considered a meaningful value.

4.6 NGC 3621

This galaxy has a stellar disc and a rotation curve of similar maximum velocity and shape as that of NGC 3198, and like that galaxy has a high surface brightness. However, the galaxy exhibits significantly more of a cusp when analysed.

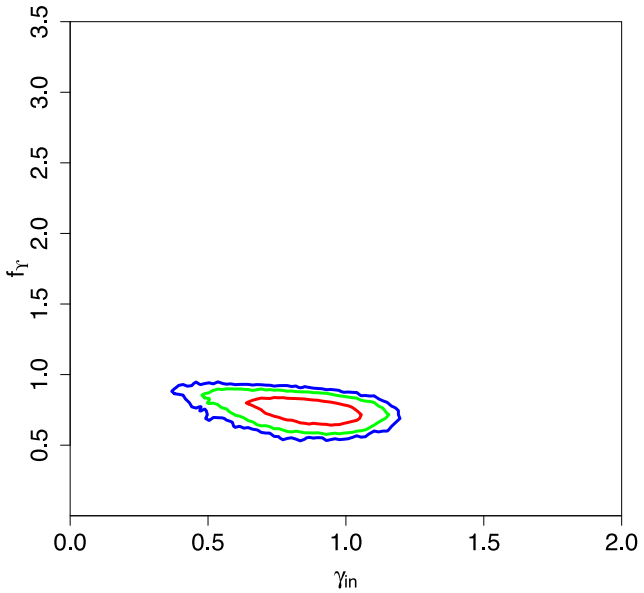

Figure 11. Contour plot of the mass-to-light multiplier f_Υ versus $\gamma_{\rm in}$ of all the models produced by the NGC 3621 MCMC run.

In Fig. 11, we see there is a slight degeneracy between $\gamma_{\rm in}$ and f_Υ. Although $\gamma_{\rm in}$ is well constrained when the mass-to-light ratio parameter varies freely (the red contour on the map showing the 1σ level, with an overall range $\gamma_{\rm in} = 0.91\pm^{0.13}_{0.33}$), or when the ratio is fixed to a particular value, the position of the distribution varies from moderately cored ($\gamma_{\rm in} = 0.33\pm^{0.31}_{0.16}$ when using a diet Salpeter IMF) to almost entirely cusped ($\gamma_{\rm in} = 0.89\pm^{0.16}_{0.2}$ when using a Kroupa IMF).

The cusped interpretation is favoured when the MCMC can control f_Υ; however, this distribution is a product of our prior assumptions. The correct value of f_Υ also needs to account for any molecular gas not included in the model, so it is difficult to give a precise value for it. We cannot at this point state which of the $\gamma_{\rm in}$ values is correct from just this analysis.

4.7 NGC 7793

NGC 7793 is another high surface brightness galaxy, but at first sight we appear to be able to constrain it reasonably well. We generated a test case for high surface brightness galaxies based on NGC 7793 in HW13.

According to Fig. 12, both the inner log slope and the mass-to-light multiplier f_Υ are well constrained and show a clearly cored profile. However, the constraint indicates a mass-to-light ratio which is substantially higher than that implied by a diet Salpeter IMF, possibly due to the involvement of molecular gas. Different values, with equally tight constraints, are found when a fixed mass-to-light ratio is chosen, as shown in Fig. 13 However, Fig. 14 shows that r_1 is well constrained, and the values for the fixed mass-to-light cases are compatible (see Table 2 below).

This demonstrates a reason why the likelihood distributions in Fig. 13 must be used with caution. Each distribution, taken in isolation, returns a very strong constraint – but it is only apparent through a broader analysis of the parameter space of the result that this constraint is entirely dependent on the initial assumption about the stellar mass-to-light ratio. This emphasizes the value of the MCMC approach.

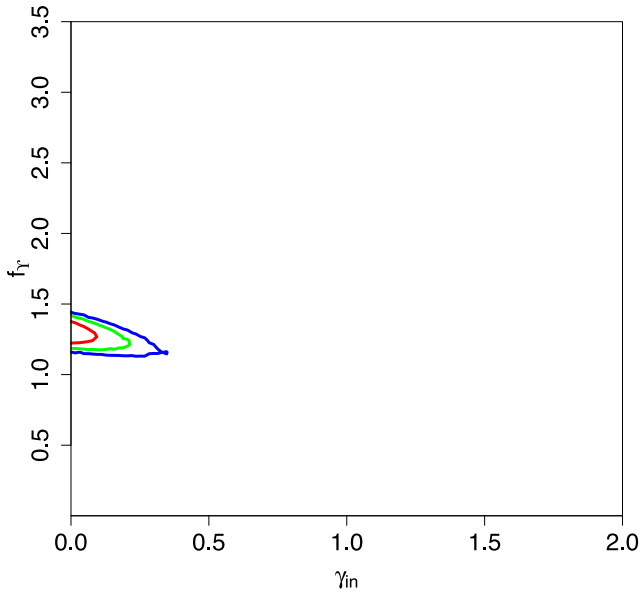

Figure 12. Contour plot of the γ value versus mass-to-light multiplier f_Υ of all the models produced by the NGC 7793 MCMC run.

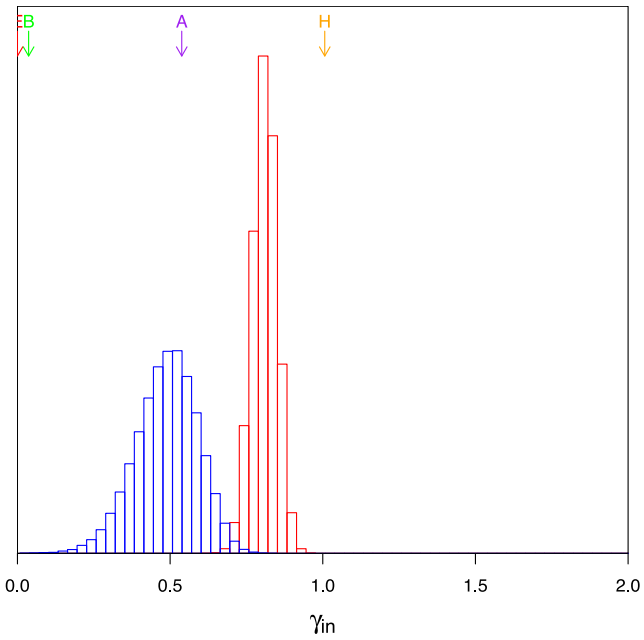

Figure 13. Histograms of γ_{in} values for NGC 7793 runs (blue) using a diet Salpeter IMF derived mass-to-light ratio, and (red) using a Kroupa IMF (Kroupa 2001) derived mass-to-light ratio. Histograms are scaled to have equal integrated area. For a Kroupa IMF, $f_\Upsilon = 0.72$ and for a diet Salpeter IMF $f_\Upsilon = 1$.

4.8 NGC 925

This galaxy is described in de Blok et al. (2008) as having a weak bar, which is found in Elmegreen, Wilcots & Pisano (1998) to have a length of 5.4 kpc. The impact of this bar on the kinematics, and thus the rotation curve, of the galaxy must be taken into account in our analysis. We do this through two separate runs of this galaxy, one with the entire data range from de Blok et al. (2008), and one

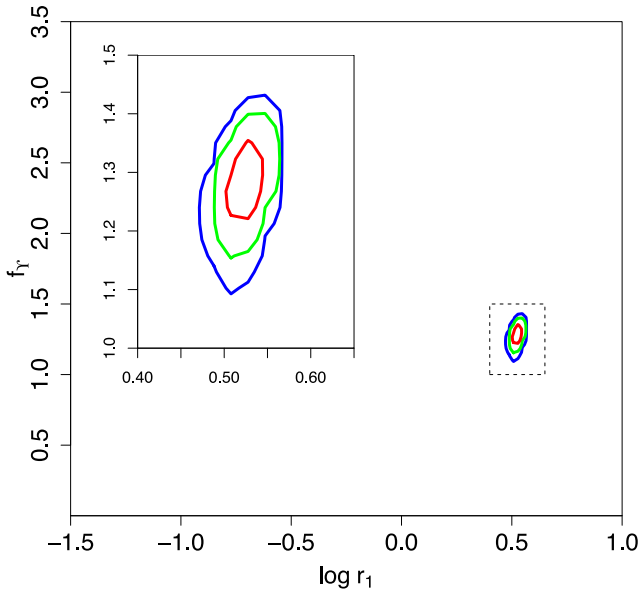

Figure 14. Contour plot of f_Υ versus r_1 for NGC 7793. Inset shows a zoom in on the contoured region.

excluding the data points inside $r = 5.6$ kpc in order to minimize the impact of bar kinematics on our result.

In a previous analysis (Chemin et al. 2011), the calculated rotation curve of this galaxy was found to be well fitted by an Einasto profile dark matter halo that featured a sharp change in the rotation curve, caused by the single Einasto shaping parameter (n in Chemin et al. 2011 but also referred to as α in Navarro et al. 2004) being very low. Such a halo was avoided in our analysis through the availability of more shaping parameters.

The fits to this halo strongly point to the existence of a core, with a radius that encompasses most of the data range. Forcing a fixed mass-to-light multiplier does not change the result, it merely reduces the size of the tail of the distributions. Assuming a diet Salpeter IMF results in a supermaximal disc, i.e. the calculated stellar contribution being higher than the observed rotation velocity, for a number of points towards the inner part of the rotation curve, so we conclude that the Kroupa IMF derived stellar component represents a more realistic fixed Υ.

As shown in Fig. 15, the contribution of the stellar component is high at small r, but the surface brightness becomes much lower further out in the disc. This could mean that the cored profile (which has the steepest rotation curve) is simply the one which allows the dark matter contribution to most quickly transition from almost irrelevant, to being the dominant contribution, as radius increases. There is also a feature at around $r = 5$ kpc that is not modelled well by either the baryons or the proposed dark matter halo, and may be related to the bar.

The above does not prevent our result being robust. The cored portion of the proposed dark matter halo extends from where the stellar contribution stops matching the shape of the observed rotation curve, through to where the dark matter contribution is dominant. So, whilst the innermost data points may not able to constrain a core, if there were not a flat density profile at these points, the overall profile would be surprising as it would have uniform density at intermediate radii, and a rising density again interior to this.

Due to the influence of the bar, and the fact that the rotation curve indicates a larger stellar contribution than that of dark matter at small r, we do not consider the log slope here itself to be evidence of a

Table 2. Table of all calculated $\gamma_{\rm in}$ and r_1 values, with 90 per cent confidence intervals. Reduced χ^2 values shown are estimates of the peak likelihood, taking the 90th percentile of a randomly selected sub-sample of $\sim 10^3$ models from the MCMC chains. The r_1 value for NGC 3521, assuming a diet Salpeter IMF, is outside of the data range, as are the confidence intervals for all r_1 values for NGC 2976. Values for NGC 2403 and NGC 3521 use a temperature $T = 2$, sampling $P^{1/2}$ rather than P. See text for detailed discussion.

	Free f_Υ			Kroupa IMF			Diet salpeter IMF		
Galaxy	r_1 (kpc)	$\gamma_{\rm in}$	$\chi^2_{\rm red}$	r_1 (kpc)	$\gamma_{\rm in}$	$\chi^2_{\rm red}$	r_1 (kpc)	$\gamma_{\rm in}$	$\chi^2_{\rm red}$
DDO154	$1.28\pm^{0.41}_{0.28}$	$0.42\pm^{0.24}_{0.15}$	0.2	$1.18\pm^{0.31}_{0.24}$	$0.43\pm^{0.23}_{0.14}$	0.2	$1.17\pm^{0.46}_{0.33}$	$0.5\pm^{0.25}_{0.21}$	0.13
NGC2976	$1.94\pm^{1.76}_{0.4}$	$0.47\pm^{0.16}_{0.38}$	0.26	$3.24\pm^{1.14}_{0.89}$	$0.09\pm^{0.26}_{0.07}$	0.32	<4.18	<0.97	0.58
NGC7793	$3.3\pm^{0.14}_{0.14}$	<0.13	0.52	$2.93\pm^{0.13}_{0.17}$	$0.81\pm^{0.06}_{0.07}$	0.67	$3.15\pm^{0.15}_{0.28}$	$0.51\pm^{0.14}_{0.18}$	0.36
NGC2403	<2.81	$0.72\pm^{0.29}_{0.49}$	0.15	$0.35\pm^{0.15}_{0.25}$	$0.8\pm^{0.2}_{0.17}$	0.29	$0.75\pm^{0.44}_{0.5}$	$0.7\pm^{0.34}_{0.26}$	0.15
NGC925	$6.76\pm^{0.46}_{0.51}$	<0.29	0.25	$7.43\pm^{0.45}_{0.4}$	$0\pm^{0.06}_{0}$	0.42	$8.4\pm^{7.99}_{0.75}$	<0.09	0.55
NGC3621	<1.44	$0.87\pm^{0.18}_{0.26}$	0.28	<0.88	$0.9\pm^{0.17}_{0.2}$	0.27	$4.61\pm^{1.04}_{1.6}$	$0.39\pm^{0.36}_{0.21}$	0.18
NGC3198	$3.33\pm^{0.14}_{0.97}$	$0.09\pm^{0.28}_{0.07}$	0.38	$4.19\pm^{0.4}_{0.7}$	$0.05\pm^{0.3}_{0.03}$	0.67	$6.36\pm^{1.6}_{1.71}$	$0.14\pm^{0.41}_{0.09}$	0.6
NGC3521	$2.02\pm^{0.36}_{0.26}$	$0.03\pm^{0.17}_{0.02}$	0.68	$3.88\pm^{1.36}_{1.2}$	$0.08\pm^{0.38}_{0.04}$	1.25	$30.58\pm^{20.74}_{12.27}$	<0.03	2.09

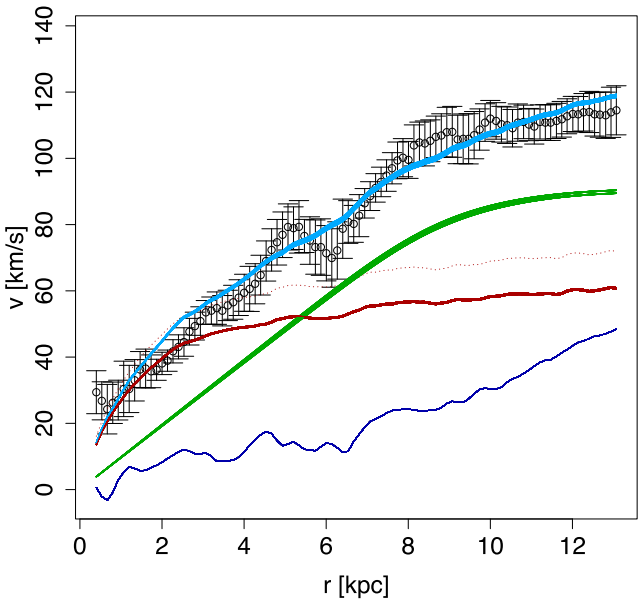

Figure 15. Rotation curve produced by the MCMC analysis of the data for NGC 925 assuming a fixed Kroupa IMF. The black data points are H I rotation curve data, the red solid line is the modelled stellar contribution derived from a Kroupa IMF to the rotation curve, the dark blue line is the modelled gas contribution, the green line is the dark matter halo model at the peak of the distribution, and the light blue line is the expected rotation curve produced by all these components. For comparison the dotted line shows the stellar component assuming a diet Salpeter IMF, which is not used in this calculation.

cored density profile. However, we note that analysis of this galaxy gives a value of $r_1 = 6.84\pm^{0.41}_{0.53}$ (90 per cent confidence interval) which places the scale radius beyond the radial extent of most of the bar.

Our second run, excluding the inner part of the rotation curve, showed $r_1 = 6.77\pm^{0.65}_{0.75}$. In this case, γ is less well constrained, as illustrated in Fig. 16. This shows that for this galaxy the r_1 result is not compromised by any relation between γ and r_1. We conclude that r_1 is well constrained for this galaxy, but $\gamma_{\rm in}$ is much less well constrained. However, it should be noted that higher values of $\gamma_{\rm in}$, associated with a cusped profile, are much more difficult to reconcile with the value we have for r_1 as it would imply a very slow change in log slope and thus provide a poor fit at larger r.

Our modelling can also explain the anomalous result obtained for this galaxy by Chemin et al. (2011). The rotation curve requires a flat log slope over a large radial range in order to produce a good fit, and the only way to do this with an Einasto halo is to lower the shape parameter n radically, which also leads to an unphysical, sharp drop in density near $r = 10$ kpc. A profile with more parameters (in this case, γ controlling the inner log slope and α controlling the rate of transition from the inner to the outer asymptotic log slopes) avoids this problem.

4.9 Rejected galaxies

We attempted to apply this technique to NGC 2841, NGC 2903, NGC 3031, NGC 4736, NGC 5055 and NGC 7331, but we found that there were either inadequate kinematic data for the MCMC algorithm to find a genuine fit to the data, or there was sufficient underlying asymmetry in the disc to prevent the MCMC method finding a useful constraint.

In the case of NGC 5055, the morphology of the galaxy and the shape of the rotation curve both appear promising as a target for this technique. However, when we applied an MCMC analysis, we were unable to constrain any parameters. In Fig. 3, we showed the peak of the distribution. The halo corresponding to the most populated bin in the parameter space fits the data well, and relying purely on the value of $\chi^2_{\rm red} < 0.5$ without the context of the parameter space, the conclusion would be that the halo has been correctly modelled.

The extra information provided by the MCMC process allows us to show that this is not the case. In Fig. 17, we see the distribution of $\gamma_{\rm in}$ values is not smooth over a length-scale comparable to the initial step size of the MCMC chain, suggesting the eight parallel chains have not converged to the same distribution, despite them visiting over $\sim 4 \times 10^7$ models between them. At temperature settings $T = 1$, 2, and 3, we were unable to produce a set of chains with a convergence statistic $\sigma(\hat{x})/\hat{\sigma}(x) < 1$ for all parameters. Without a repeatable probability distribution, we cannot draw any conclusions.

5 DISCUSSION

Our MCMC method has produced good constraints on r_1 in those galaxies where such a constraint is possible. We now place these estimates in the context of other work, and then use the model we

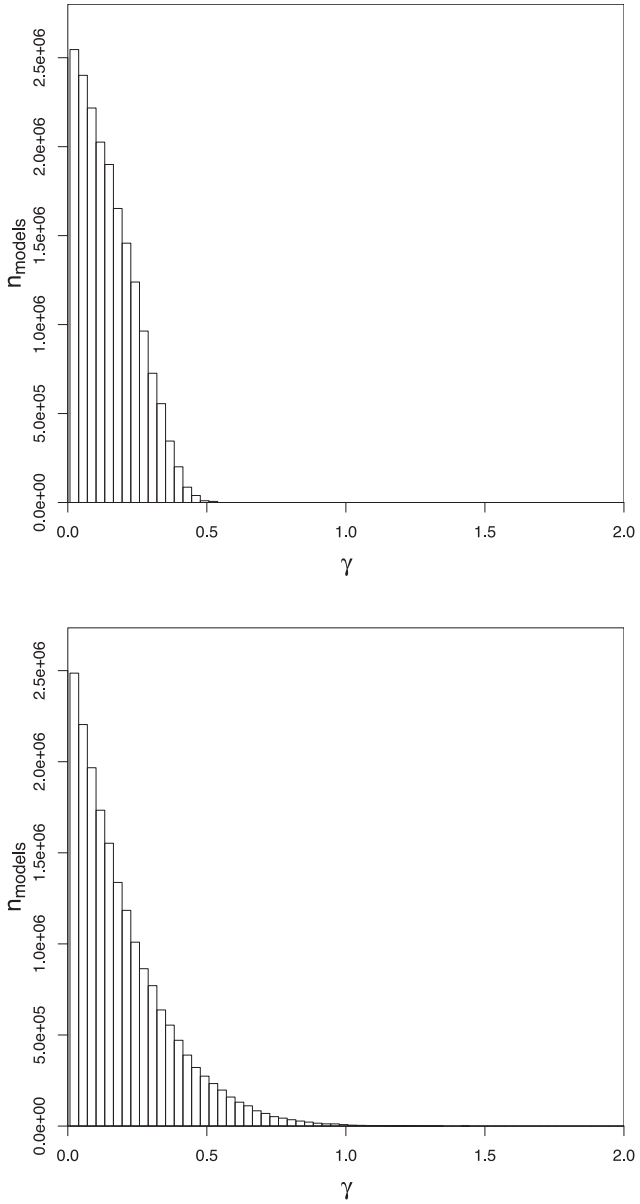

Figure 16. Distributions of γ for NGC 925 using all data points (top) and using only those data points outside $r_1 = 6.77$ (bottom). Note that we do not use $\gamma_{\rm in}$ for this comparison as the two cases have different inner radial bins. See text for a discussion.

outlined in Section 3 in order to explore what we can deduce about their formation history.

5.1 Scalelength correlation

In Donato et al. (2004), it is suggested that, for a set of 25 galaxies, the scalelength of the dark matter halo is proportional to the scalelength of the stellar disc. The cored density profile used to argue for proportionality with the disc scale is a pseudo-isothermal halo, given by

$$\rho(r) = \rho_0 \frac{r_{\rm c}^2}{r^2 + r_{\rm c}^2} \tag{7}$$

and the stellar component is modelled by an exponential disc with a scalelength $R_{\rm D}$. The profile (7) does not show the same degeneracy between ρ_0 and $r_{\rm c}$ as the $\alpha-\beta-\gamma$ profile, because it becomes independent of $r_{\rm c}$ at small radii. However, it is effectively a single parameter profile. In our analysis, we have found that $v_{\rm max}$ is strongly constrained, and this constraint translates into a constraint on $\rho_0 r_{\rm c}^2$ at large radii. Therefore, for any given value of ρ_0 (which controls the core behaviour on its own) there is little freedom in $r_{\rm c}$. This in itself does not imply that $r_{\rm c}$ is necessarily meaningless, so we have investigated whether or not there is an equivalent correlation to that found in Donato et al. (2004) in the galaxies we are examining.

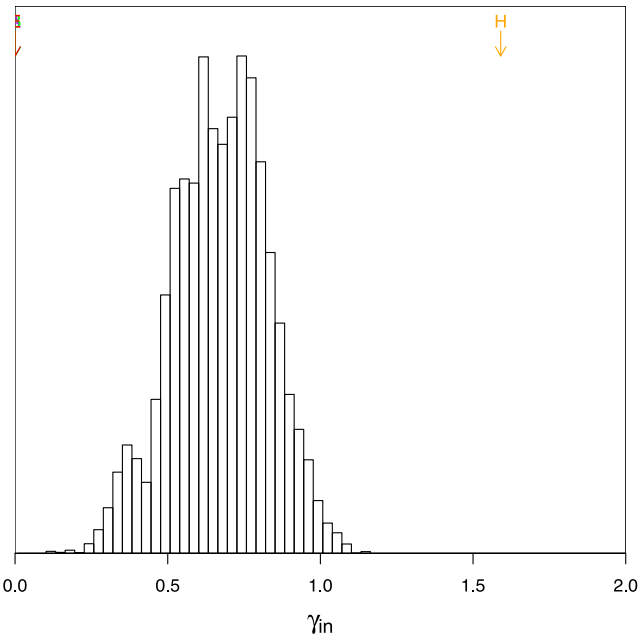

Figure 17. Histogram of $\gamma_{\rm in}$ values from an MCMC run on NGC 5055 with a temperature setting $T = 1$. There are $\sim 4 \times 10^7$ models included from eight independent chains. Arrows are as in Fig. 4.

In order to exclude the possibility of the reported correlation being an artefact, we generated sets of 100 rotation curves with random, uncorrelated scale radii for the stellar disc and dark halo of $R_{\rm d} = 3 \pm 1$ kpc and $r_{\rm s} = 5 \pm 2$ kpc, respectively. We added Gaussian noise to the data and included 1σ error bars of the corresponding size. The dark halo models were either Burkert, pseudo-isothermal, or NFW. We then found the best-fitting pseudo-isothermal haloes, given a free mass-to-light ratio. In none of the cases did we find a correlation. Give that Donato et al. (2004) found that maximal discs were favoured in their models, we then forced a maximal disc to be used before fitting the pseudo-isothermal halo. Again, we did not find a correlation.

We investigated whether there is a comparable correlation from our own data set (shown in Fig. 18), by assuming a maximal disc and fitting a single pseudo-isothermal profile to each galaxy. We do not see a relation as presented in Donato et al. (2004), although we note that our sample is smaller and has a narrower range of properties. It should also be noted that in order to produce maximal disc fits, higher f_Υ values than we allowed in our MCMC modelling had to be assumed in many cases.

5.2 Feedback modelling

The question of whether or not there is a relation between any parameters of the baryonic component of a galaxy and parameters

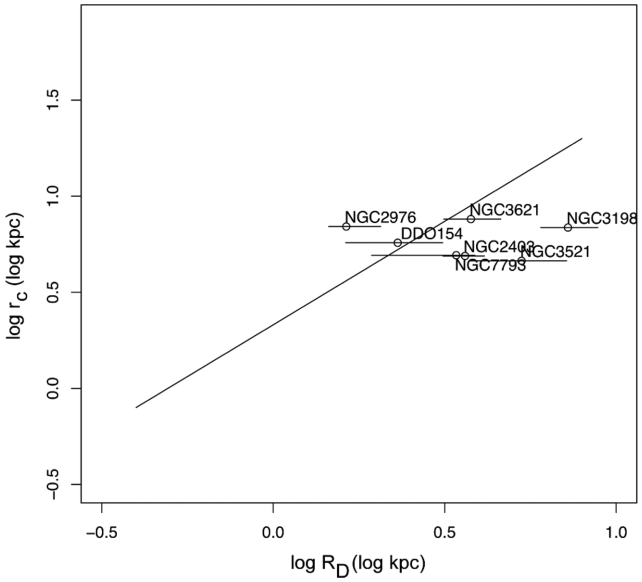

Figure 18. The relation between the dark matter core radii, as defined in equation (7) and stellar disc radii for our set of galaxies assuming a cored pseudo-isothermal halo profile. NGC 925 is off the right-hand edge of this plot. The overlaid solid line is the relation identified by Donato, Gentile & Salucci (2004).

of its dark matter halo is relevant to understanding galaxy formation. It is presumed, based on cosmological models by Navarro et al. (1996) and others, that the centres of dark matter haloes begin strongly cusped, and then become cored by some interaction with baryonic matter (e.g. Governato et al. 2010).

The r_1 parameter we calculate can be used to gain some insight into this. Any process which reshaped the halo must be able to disrupt the potential of the galaxy to at least this radius, under the assumptions of an NFW starting point and a spherically symmetric halo. In Table 2, we show that for galaxies DDO 154, NGC 2403 and NGC 2976, the values of r_1 are for each galaxy within the 90 per cent confidence intervals of each other for all prior assumptions about mass-to-light ratio used here. In the case of NGC 7793, the intervals do not entirely overlap but, as Fig. 14 shows, the constraint on r_1 is very strong and not dependent on f_Υ so this is not an issue of baryonic modelling.

We now focus on DDO 154, the smallest galaxy in our set, because work such as Governato et al. (2010) focuses on feedback in dwarf galaxies. Considering supernova feedback, if each 100 $M_\odot$ of star formation leads to a single supernova which feeds back 10^{44} J of energy ($5.6 \times 10^{-6} M_{\rm intial}$ equivalent solar masses), and assuming the current stellar mass is ≈88 per cent of the initial mass (using a Kroupa IMF gives an initial composition where 12 per cent of the total stellar mass is O stars (Kroupa 2001), and have all undergone supernova), the feedback energy is 210 $M_\odot c^2$. This is larger than the energy change required in the dark matter halo to modify its density profile; the difference in total kinetic energy between DDO 154 and the closest NFW halo (based on least squares fitting) is $1.2 \pm^{1.6}_{0.9}$ $M_\odot c^2$. Energy production is in this galaxy therefore does not constrain this process, so we must focus on how this energy can be transferred to the dark matter halo.

Feedback from a central star forming region in DDO 154 was modelled in Gelato & Sommer-Larsen (1999) as an attempt to explain the discrepancy between observations of the galaxy and the NFW halo model. They were only able to reproduce the observed rotation curve by assuming a disc more massive than that which is observed in H I emissions, and furthermore Read & Gilmore (2005) shows that their method of contracting the dark matter halo cusp could bias its final state after outflow towards being more flat, due to the assumed isotropic velocity structure of the halo. Applying the method described in Section 3 to DDO 154, we find a gas fraction available for feedback $f_{\rm g} = 0.42$, compared to the estimate of the currently observed baryon fraction of 0.1 by Carignan & Purton (1998), which supports the conclusion that this galaxy requires additional baryonic mass to account for its dark matter halo profile (although it still leaves open the question of where this mass is now). The complete set of values for $f_{\rm g}$, for all the galaxies studied here, are shown in Table 3.

Table 3. Inferred available gas fractions at the time of outflow, based on a simple spherical model, along with $\gamma_{\rm in}$ values taken from the free f_Υ case. Note that $M_{\rm I,\,gas}$ here refers to the baryon mass interior to r_1, so $f_{\rm g}$ is a factor 2 smaller than the total mass deficit.

Galaxy	$M_{\rm F,\,dark}/(M_{\rm I,\,dark} + M_{\rm I,\,gas})$	f_g	$\gamma_{\rm in}$
DDO 154	0.16	0.42	$0.42\pm^{0.24}_{0.15}$
NGC 2976	0.67	0.17	$0.47\pm^{0.16}_{0.38}$
NGC 7793	0.67	0.17	<0.13
NGC 2403	0.22	0.39	$0.72\pm^{0.29}_{0.49}$
NGC 925	0.53	0.24	<0.29
NGC 3621	0.15	0.43	$0.87\pm^{0.18}_{0.26}$
NGC 3198	0.33	0.34	$0.09\pm^{0.28}_{0.07}$
NGC 3521	0.77	0.12	$0.03\pm^{0.17}_{0.02}$

Our calculated values for $f_{\rm g}$ are minima, as the contraction of the baryonic component prior to outflow can only increase the dark matter content interior to r_1, and thus require a greater amount of gas outflow to remove. If we assume that the process of contracting dark matter through baryon motion has efficiency of order unity for infall as well as for outflow (that is, each unit mass of baryons moved past r_1 in either radial direction brings with it a unit mass of dark matter) then significant infall and contraction would move the value of $f_{\rm g}$ towards 0.5.

In Fig. 19, we show the values from Table 3 in the context of the output from the simulations in Section 3. The construction of the analytical model forces all the galaxies on to one straight line of the plot, so this should not be taken as a physical confirmation of the simulations. The simulations are shown to be consistent one of the main assumptions of the analytical model; that the amount of dark matter removed during an outflow is comparable to the amount of gas removed.

The disc of DDO 154 is dominated by neutral hydrogen gas, whose presence must be accounted for when suggesting an energetic outflow (Carignan & Purton 1998). Zubovas, King & Nayakshin (2011) present a simulated model of the Fermi bubbles above and below the disc of the Milky Way, detected in γ rays- (Su, Slatyer & Finkbeiner 2010). These bubbles are part of a black hole outflow that is pinched in the centre due to the density of the gas in the galactic disc. A black hole outflow scenario is compatible with the gas-richness of DDO 154's disc if the density of that gas is high enough that an outflow able to reach r_1 would not significantly disturb it. If we assume that the density of the dark matter halo can be approximated as $\rho \propto r^{-1/2}$ inside r_1 (as an average log slope, assuming the halo becomes flat at $r = 0$), and that the disc density

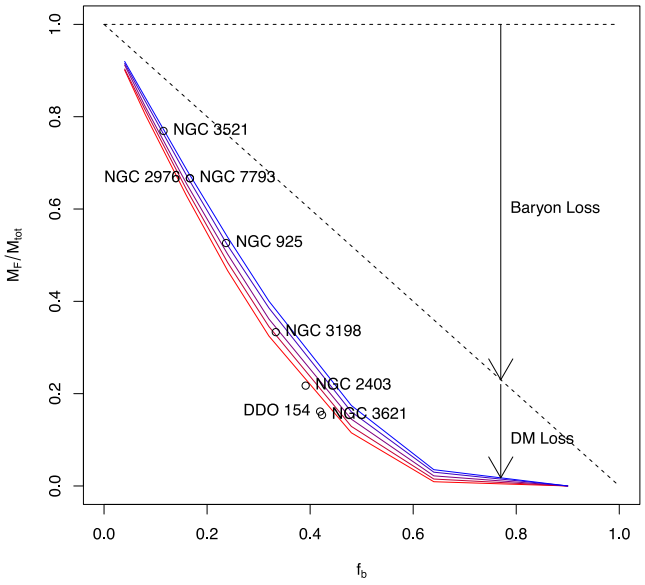

Figure 19. Comparison of data from Table 3 with simulated predictions. $M_{\rm tot} = M_{\rm I} + M_{\rm b}$ is the total mass, baryons and dark matter, interior to r_1. The dotted line shows the remaining mass after baryon removal, and the solid lines show the overall mass-loss after 1 Gyr for various halo profiles. As in Fig. 1, red to blue denotes increasing log slope (0, 0.25, 0.5, 7/9, 1). Simulations were run for baryon fractions $f_{\rm b} = 0.02, 0.04, 0.08, 0.16, 0.24, 0.48, 0.64, 0.90$. The positions of the galaxies are determined by the analytical model, which always assumes equal baryon and dark matter loss and thus they must all lie on in a single line. The simulation results are not by construction forced to agree with the analytical results. Vertical arrows illustrate the decrease in mass due to the baryon loss (simulated by reduction of particle masses) and the resultant decrease in dark mass.

can also be approximated near the centre of the galaxy by a $\rho \propto r^{-1/2}$ profile, the energy required to lift all matter inside r_1 to r_1 is

$$U = \frac{3}{5}\frac{GM(r_1)^2}{r_1}. \tag{8}$$

Imparting the same amount of energy to both components, and cancelling the enclosed mass of both components, gives

$$\frac{M_{\rm halo}(r_1)}{r_1} = \frac{M_{\rm disc}(R_{\rm outflow})}{R_{\rm outflow}}, \tag{9}$$

where $R_{\rm outflow}$ is the distance gas can be swept up in the disc with the same energy required to sweep up all halo gas to r_1. For the $\rho = \rho_0(\frac{r}{r_0})^{-1/2}$ density profile we use,

$$M = 4\pi\int_0^r \rho(r')r^2{\rm d}r = \frac{8}{5}\pi\rho_0 r^{5/2}r_0^{2/3} \tag{10}$$

assuming equal scale radii and substituting into equation (9), we can calculate how an outflow that sweeps up all gas to a specific radius would travel in the two different media

$$R_{\rm outflow} = \left(\frac{\rho_{0,\rm halo}}{\rho_{0,\rm disc}}\right)^{2/3} r_1. \tag{11}$$

Taking the model of Banerjee et al. (2011) for the inner regions of the gas disc of DDO 154, with a pseudo-isothermal scale density of dark matter $\rho_{\rm dm} = 0.028\,{\rm M}_\odot\,{\rm pc}^{-3}$, $\Sigma_{\rm H\,I} = 5.7\,{\rm M}_\odot\,{\rm pc}^{-3}$, and gas scaleheight $h = 100\,{\rm pc}$ from Banerjee et al. (2011), we derive $\rho_{0,\rm halo} = 4.8\times10^{-3}\,{\rm M}_\odot\,{\rm pc}^{-3}$ and $\rho_{0,\rm disc} = 0.057\,{\rm M}_\odot\,{\rm pc}^{-3}$. We use the halo model of Banerjee in this calculation because their disc model is calculated assuming a pseudo-isothermal halo – however, our rotation curve data are the same. Given the value $r_1 = 1.21\,{\rm kpc}$ for DDO 154, we therefore estimate $R_{\rm outflow} = 192\,{\rm pc}$. The first radial bin in this galaxy is situated at $R = 135\,{\rm pc}$, which means a Fermi bubble-like outflow cannot be excluded based on the presence of gas in the disc.

6 CONCLUSIONS

We have applied the MCMC method described in HW13 to a number of nearby galaxies and been able to constrain the density profiles of their haloes with less ambiguity than would be possible with simpler statistical methods. From these constraints, we have determined that the sample of galaxies studied here cannot be described by a single, universal, halo profile. We have also calculated from the modelled haloes the values of physical quantities (r_1 and $f_{\rm g}$) which can be used to constrain formation scenarios for these galaxies.

Contrary to work such as Kuzio de Naray et al. (2008) and Chemin et al. (2011), we find that a lower reduced χ^2 value does not necessarily indicate a better description of the data. Their assertion requires the errors be correct, and that the degrees of freedom be constant across the parameter space, neither of which is necessarily correct for these data and these models. Our MCMC method only relies on the χ^2 values being locally meaningful for consecutive members of the Markov chain, and the use of a more general profile removes the strong prior link between the inner and outer haloes imposed by other profiles such as NFW.

The sample investigated here is subject to a selection bias. The THINGS galaxies were subsampled for generation of rotation curves by de Blok et al. (2008), based on inclination and other factors, and then subsampled again here on the basis of whether or not they can produce meaningful outputs from our MCMC technique. Our conclusions must be interpreted in this context.

The selection biases we experience also apply to any attempt at rotation curve decomposition. The cases where MCMC cannot find a constraint should be taken as an indication that the fitting of an individual profile, that is part of our parameter space or closely approximated by a profile that is, cannot produce a result that is credible without further discussion of the issues that prevent a constraint with MCMC. Our technique has the potential to overcome these bias using different data, or different modelling of the data (that incorporates more well-constrained stellar populations for instance). The behaviour of our MCMC technique with potential future data sets is described in HW13 and is found to be promising.

We have identified several degeneracies in the parameter space. Some we are unable to break, such as the degeneracy between Υ and the inner log slope $\gamma_{\rm in}$ for NGC 3621. One of the most important degeneracies we discovered is between $\rho_{\rm s}$ and $r_{\rm s}$, which has been resolved in all cases presented here. This degeneracy precludes these two parameters being independently considered as physical. Our transformation of the parameter $\rho_{\rm s}$ into $v_{\rm max}$ removes this degeneracy, but unfortunately $r_{\rm s}$ still cannot be interpreted as a physically meaningful radius, because its position is degenerate with the shaping parameters α, β and γ.

Scale radii fixed by the points at which the curve reaches a particular log slope (i.e. r_n where n is the negative log slope) are more useful for a discussion of the actual morphology of dark matter haloes. We chose r_1 due to the fact that parts of the halo interior to this distance cannot be modelled by a cosmological halo such as NFW. Thus, r_1 corresponds to a radius over which baryonic physics must act in order to produce the measured halo.

We have shown that r_1 is useful and well constrained, and that it can be used to constrain a simple feedback-based formation model. The relevance of r_1 is first as a constrainable physical parameter

within the data range of the galaxies studied here, secondly as a required scale of mass-loss (under reasonable assumptions) and thirdly as a common scaling parameter with which to compare observationally derived haloes to simulated ones in a physically meaningful way. The second reason applies only for r_1 and not for other radii. However, we recognize that other radii may have similar uses, and such radii may also be constrained well with an MCMC method, as we have used here.

The model we use to derive f_g is simple, but links a physically viable outflow scenario to a quantity derived by MCMC analysis of observations, and could be refined iteratively by using it as an initial condition in formation simulations. This value cannot be reliably derived from simpler fitting methods due to the complexity of the parameter space, and the low quality of measures such as χ^2_{red} as absolute goodness of fit statistics for these data. MCMC provides a firm enough constraint, and a confidence that the parameter space has been properly explored, to allow results such as f_g to guide simulations.

ACKNOWLEDGEMENTS

This work made use of THINGS, 'The HI Nearby Galaxy Survey' (Walter et al. 2008). This work is based [in part] on observations made with the *Spitzer* Space Telescope, which is operated by the Jet Propulsion Laboratory, California Institute of Technology under a contract with NASA. We would like to thank Walter Dehnen, Albert Bosma and Martin Bourne for valuable discussions. The COSMOMC code was written by Anthony Lewis (Lewis & Bridle 2002). We would also like to thank Erwin de Blok for providing model data (de Blok et al. 2008) in electronic format. MIW acknowledges the Royal Society for support through a University Research Fellowship. PRH acknowledges STFC for financial support. This research used the Complexity HPC cluster at Leicester which is part of the DiRAC2 national facility, jointly funded by STFC and the Large Facilities Capital Fund of BIS.

REFERENCES

Banerjee A., Jog C. J., Brinks E., Bagetakos I., 2011, MNRAS, 415, 1, 687
Begeman K. G., 1989, A&A, 223, 47
Bell E. F., de Jong R. S., 2001, ApJ, 550, 212
Binney J., Tremaine S., 2008, Galactic Dynamics, 2nd edn, Princeton Series in Astrophysics. Princeton Univ. Press, Princeton, NJ
Bosma A., 1978, PhD thesis, Groningen Univ.
Bosma A., 2003, Rev. Mex. Astron. Astrofis. Conf. Ser., 17, 15
Bullock J. S., Kolatt T. S., Sigad Y., Somerville R. S., Kravtsov A. V., Klypin A. A., Primack J. R., Dekel A., 2001, MNRAS, 321, 559
Burkert A., 1995, MNRAS, 447, 1
Carignan C., Purton C., 1998, ApJ, 506, 125
Chemin L., de Blok W. J. G., Mamon G. A., 2011, AJ, 142, 109
de Blok W. J. G., Bosma A., McGaugh S., 2003, MNRAS, 340, 657
de Blok W. J. G., Walter F., Brinks E., Trachternach C., Oh S.-H., Kennicutt R. C., Jr, 2008, AJ, 136, 2648
Dehnen W., 2000, ApJ, 536, L39
Dehnen W., 2002, J. Comput. Phys., 179, 27
Donato F., Gentile G., Salucci P., 2004, MNRAS, 353, L17
Dubinski J., Carlberg R. G., 1991, ApJ, 378, 496
Elmegreen B. G., Wilcots E., Pisano D. J., 1998, ApJ, 494, L37
Gelato S., Sommer-Larsen J., 1999, MNRAS, 303, 2, 321
Gentile G., Salucci P., Klein U., Vergani D., Kalberla P., 2004, MNRAS, 351, 903
Governato F. et al., 2010, Nature, 463, 203
Hague P. R., Wilkinson M. I., 2013, MNRAS, 433, 2314 (HW13)
Hastings W. K., 1970, Biometrika, 57, 1, 97
Katz H., McGaugh S. S., Sellwood J. A., de Blok W. J. G., 2014, MNRAS, 439, 1897
Kennicutt R. C., Jr et al., 2003, PASP, 115, 928
King A., 2003, ApJ, 596, L27
Kroupa P., 2001, MNRAS, 322, 231
Kuzio de Naray R., McGaugh S. S., de Blok W. J. G., 2008, ApJ, 676, 920
Leroy A. K., Walter F., Bigiel F. et al., 2009, AJ, 137, 4670
Lewis A., Bridle S., 2002, Phys. Rev. D, 66, 103511
Navarro J. F., Frenk C. S., White S. D. M., 1996, ApJ, 462, 563
Navarro J. F. et al., 2004, MNRAS, 349, 1039
Oh S.-H., de Blok W. J. G., Brinks E., Walter F., Kennicutt R. C., Jr, 2011, AJ, 141, 193
Read J. I., Gilmore G., 2005, MNRAS, 356, 107
Su M., Slatyer T. R., Finkbeiner D. P., 2010, ApJ, 724, 1044
Trachternach C., de Blok W. J. G., Walter F., Brinks E., Kennicutt R. C., Jr, 2008, AJ, 136, 2720
van den Bosch F. C., Swaters R. A., 2001, MNRAS, 325, 1017
Walter F., Brinks E., de Blok W. J. G., Bigiel F., Kennicutt R. C., Jr, Thornley M. D., Leroy A., 2008, AJ, 136, 2563
Zhao H., 1996, MNRAS, 278, 488
Zubovas K., King A. R., Nayakshin S., 2011, MNRAS, 415, L21

This paper has been typeset from a TEX/LATEX file prepared by the author.